Published in final edited form as:
Biomaterials. 2013 January ; 34(1): 42–54. doi:10.1016/j.biomaterials.2012.09.053.

Photopolymerized microfeatures for directed spiral ganglion neurite and Schwann cell growth

Bradley W. Tuft[a], **Shufeng Li**[b,c], **Linjing Xu**[b], **Joseph C. Clarke**[b], **Scott P. White**[a], **Bradley A. Guymon**[b], **Krystian X. Perez**[a], **Marlan R. Hansen**[b], and **C. Allan Guymon**[a]

[a]Department of Chemical and Biochemical Engineering, University of Iowa, Iowa City, IA 52242, USA

[b]Department of Otolaryngology, University of Iowa Hospitals and Clinics, Iowa City, IA 52242, USA

[c]Department of Otolaryngology, Eye & ENT Hospital of Fudan University, Shanghai, 200031, China

Abstract

Cochlear implants (CIs) provide auditory perception to individuals with severe hearing impairment. However, their ability to encode complex auditory stimuli is limited due, in part, to poor spatial resolution caused by electrical current spread in the inner ear. Directing nerve cell processes towards target electrodes may reduce the problematic current spread and improve stimulatory specificity. In this work, photopolymerization was used to fabricate micro- and nano-patterned methacrylate polymers to probe the extent of spiral ganglion neuron (SGN) neurite and Schwann cell (SGSC) contact guidance based on variations in substrate topographical cues. Micropatterned substrates are formed in a rapid, single-step reaction by selectively blocking light with photomasks which have parallel line-space gratings with periodicities of 10 – 100 μm. Channel amplitudes of 250 nm – 10 μm are generated by modulating UV exposure time, light intensity, and photoinitiator concentration. Gradual transitions are observed between ridges and grooves using scanning electron and atomic force microscopy. The transitions stand in contrast to vertical features generated via etching lithographic techniques. Alignment of neural elements increases significantly with increasing feature amplitude and constant periodicity, as well as with decreasing periodicity and constant amplitude. SGN neurite alignment strongly correlates ($r = 0.93$) with maximum feature slope. Multiple neuronal and glial types orient to the patterns with varying degrees of alignment. This work presents a method to fabricate gradually-sloping micropatterns for cellular contact guidance studies and demonstrates spatial control of inner ear neural elements in response to micro- and nano-scale surface topography.

Keywords

Photopolymerization; Micropatterning; Surface topography; Nerve Guide; Neural Prosthesis

1. Introduction

Neural prosthetics are intended to replace or substantially augment motor and sensory functions of neural pathways that have been lost or damaged due to physical trauma,

disease, or genetics. Ongoing developments in the fields of neurobiology, materials science, and tissue engineering are enabling innovative device designs and modifications that may considerably expand the functional potential of such complex medical devices. However, much of this functional potential remains unrealized due to poor host tissue integration that significantly limits the performance of most neural prostheses[1].

In particular, neural prosthetic performance is limited by low spatial signal resolution at the neural-electrode interface[2,3]. Consequently, prostheses fail to recapitulate the intimate, precise interactions inherent to neural networks and therefore fail to provide precise motor or sensory stimulation. For example, visual resolution provided by retinal prostheses is limited to few sensory pixels, at least in part, by electrical signal overlap caused by spatial separation of stimulating electrodes from the target neurons in the retina [3]. Similarly, the cochlear implant (CI) enables basic auditory perception to individuals with severe hearing loss but provides limited tonal information due to comparable limitations in spatial signal control. For CIs, spatial limits to tonal fidelity occur due to electrical signal spread across the neural-electrode interface that excites neurons which are outside of the preferred area of stimulation. As a result, non-specific signaling causes CI patients to struggle with complex auditory stimuli such as music appreciation, voice comprehension in environments with noise, and voice intonations[4,5]. Furthermore, because the nervous system is generally dependent upon signaling that is location specific, analogous signal resolution challenges are expected for all devices that interact with the nervous system. Precise spatial signal control will, therefore, be critical to achieve significant performance improvements in next-generation neural-prosthetics.

To address spatial resolution challenges, significant research interest has focused on guiding sensory neurites to approach or even contact prosthesis electrodes [2,6–12]. Spatial proximity to stimulating electrodes would allow for lower stimulation thresholds that would reduce problematic signal overlap, enable higher stimulatory specificity, and perhaps lead to greater precision in both signal input and biological functional output. Recent research illustrates a variety of methods used to direct the outgrowth of regenerative neural processes, including aligned microfibers[13], parallel micro- and nano-channel morphology[14,15], axonal conduits[16], cyto-mimetic patterning[17], bioactive molecule patterning[18–21], diffusion gradients of chemo-attractants[22], and electrical fields[23,24]. However, the principle focus of many of these studies is to induce neurites, particularly those of the sciatic nerve, to optimally extend in one direction to bridge large gaps typical of nerve injuries. Using similar guidance techniques may also be advantageous to address spatial resolution challenges at the neural-prosethetic interface by enabling spatial control of regenerative sensory neurites specific to the prosthesis.

Among the various methods used to direct cell growth, controlling cell-material interactions based on surface topography, or contact guidance, is of particular interest due to the stability, reproducibility, and high degree of control over surface physical features via well-established micro- and nano-scale patterning techniques. Additionally, contact guidance is a versatile technique used to induce specific morphologies of multiple cell types, including epithelial cells[25], fibroblasts[26], stem cells[27], osteoblasts[28], as well as neuronal and glial cells[29]. In addition to controlling cell morphology, contact guidance has also been

shown to regulate gene expression that may be advantageous for neural regeneration. For example, Schwann cells increase neurotrophin expression when cultured on microgrooved chitosan and poly(D,L-lactide) compared to those grown on smooth substrates[30]. Micropattern dimensions such as ridge width, groove depth, and pattern shape can be tuned to influence cellular outgrowth and spatial orientation as well[31,32]. Consequently, recent neural contact guidance studies inspire confidence that neuritic processes relevant to current or developing prosthetics, such as those of spiral ganglion neurons (SGNs) or retinal ganglion neurons, may be spatially oriented towards stimulating electrodes for increased signal specificity and enhanced prosthetic performance.

Accordingly, in this study, we show that photopolymerization enables facile and rapid generation of micro- and nano-patterned methacrylate substrates for contact guidance studies and also demonstrate the extent to which inner ear neural elements, namely SGN neurites and spiral ganglion Schwann Cells (SGSCs), spatially orient to 3D topographical cues. We have previously reported that SGNs and SGSCs adhere to and survive on copolymer methacrylates similar to those used for this study[33]. Micropattern feature spacing is controlled using Ronchi rule optics with varied band-spacing as photomasks and feature amplitude is tuned by terminating the reaction at specific time increments to temporally arrest amplitudes as they develop throughout the reaction. Feature amplitude is also tuned by modulating photoinitiator concentration and UV light intensity. Gradually sloping features produced by this method stand in contrast to the majority of contact guidance studies that use lithographic procedures which produce features with defined vertical edges[30,34]. Variations in the extent of SGN neurite and SGSC alignment are demonstrated using gradually sloping, parallel ridge-groove patterns that have periodicities of 10 – 50 μm and amplitudes of 250 nm – 8 μm. Alignment behavior of astrocytes (ACs) as well as neurites from dorsal root ganglion neurons (DRGNs), trigeminal neurons (TGNs), and cerebellar granular neurons (CGNs) serve as glial and neuronal comparisons, respectively. The extent of neurite alignment is also shown to strongly correlate with maximum feature slope.

2. Materials and Methods

2.1 Glass slide pretreatment

Standard 2.54 cm × 7.62 cm glass microscope slides were functionalized with a methacrylated silicon bonding agent to prevent delamination of polymer substrates from the glass during sample characterization and cellular studies. The slides were first treated under vacuum with O_2 plasma for 3 min at 30 W RF power (PDC-001 Harrick Plasma Expanded Cleaner, Ithaca, NY). Immediately following removal from the plasma chamber, the slides were immersed in a 1/100 v/v solution of 3-(trimethoxysilyl)propyl methacrylate (Aldrich) and n-hexane (Aldrich) overnight in a covered container at room temperature (~21°C). Upon removal, each slide was rinsed with fresh hexanes and allowed to dry in a fume hood before being placed in a sealed container. Functionalized slides were observed to have a slightly translucent appearance following the hexane rinse. The slides were immediately used as a substrate for polymerization when removed from the sealed container.

2.2 Micropatterned substrate fabrication

Monomer mixtures of 40 wt% hexyl methacrylate (HMA, Aldrich) and 59 wt% 1,6 – hexanediol dimethacylate (HDDMA, Aldrich) were prepared with 1 wt% of 2,2-dimethoxy-2-phenylacetophenone (DMPA, BASF) as the photoinitiator unless otherwise specified. A sample volume of 20 μL was pipetted onto the center of a functionalized glass slide and was subsequently covered with a 2.54 cm × 2.54 cm glass-chrome Ronchi rule photomask (Applied Image Inc., Rochester, NY) for patterned samples, or with a cut untreated glass slide of the same dimensions for unpatterned samples. Pre-polymer formulations spread evenly under the photomasks due to capillary forces. Polymer samples were cured with a high-pressure mercury vapor arc lamp (Omnicure S1500, Lumen Dynamics, Ontario, Canada) at a 365 nm light intensity of 16 mW/cm^2. The curing module had an 8 mm diameter liquid light guide that was equipped with an 8 mm aperture × 50 mm length beam homogenizing fused silica light pipe (Edmund Optics). A collimating lens (RLQ-1, Asahi Spectra) was attached to the end of the light guide. UV radiation was shuttered at specific times. Following polymerization, photomasks were removed from polymer surfaces and samples were washed with 95% ethanol to remove all residual monomer. Samples were allowed to air dry before use.

2.3 Micropattern characterization

2.3.1 White Light Interferometry—Micropattern periodicity and absolute channel amplitude were measured by white light interferometry (Dektak Wyko 1100 Optical Profiling System, Veeco). Channel amplitude was reported as the difference between the maximum ridge value and the adjacent minimum groove value. Average feature height was determined by measuring channel amplitude in nine different areas across each sample (n = 3 or more). Periodicity was measured as the distance between the highest points on adjacent ridges and was consistent with photomask band spacing. 2D profiles and 3D images were generated using *Vision* software associated with the instrument.

2.3.2 Scanning Electron Microscopy—Patterned polymer morphology was examined by scanning electron microscopy (SEM, S-4800, Hitachi). For top down images, patterned samples were mounted with the glass side down on aluminum SEM stubs using conductive silver paint. For cross-sectional images, glass substrates and patterned polymers were fractured and then mounted vertically on specimen stages. The SEM specimen stage was angled using an automated stage and software controls to capture angled cross-sectional images. Prior to examination by SEM, each polymer surface was sputter coated with gold. Electron accelerating voltage was set at 2 kV.

2.3.2 Atomic Force Microscopy—The slope between grooves and ridges was determined by atomic force microscopy (AFM, Asylum Atomic Force Microscope, Asylum Research). A microscope cantilever with a force constant of 46 N/m and a tuning frequency of 316.62 kHz was used. Samples were scanned at a rate of 5 μm/s with 512 points taken per scan line across 50 μm. X and Y position data were obtained from the instrument software from 2D profiles (n = 3) taken at different locations on pattern surfaces. Average and maximum slopes were calculated from profile data.

2.4 Cell Culture

Dissociated spiral ganglion (SG) cultures from P3–5 rat pups were prepared as previously described[35,36]. Dissociated dorsal root ganglion neuron (DRGN), trigeminal ganglion neuron (TGN), and cerebellar granular neuron (CGN) cultures were prepared by modification of the SG culture method. Briefly, pooled DRG or TG from P3–5 rat pups were dissociated with 0.125% trypsin and 0.1% collagenase for 45 min at 37°C, followed by gentle trituration through fire-polished glass pipettes. For CGN cultures, cerebellar cortices were collected from P3–5 rat pups, stripped of arachnoid membranes, and treated with 0.05% trypsin for 12 min at 37°C followed by gentle trituration. Astrocyte (AC) cultures were prepared and maintained from postnatal cerebral cortex according to the modification of a previously described method [37,38]. All neurons were plated on polymer substrates coated with poly-L-ornithine (100 μg/ml) and laminin (20 μg/ml).

SGN cultures were maintained in Dulbecco's Modified Eagle Medium (DMEM) supplemented with N2 additives, 5% fetal bovine serum, neurotrophin-3 (NT-3, 50 ng/ml) and brain derived neurotrophic factor (BDNF, 50 ng/ml). TGN and DRGN cultures were maintained in Neurobasal-A medium with B-27 (Invitrogen) and nerve growth factor (NGF, 50 ng/ml). CGN cultures were maintained in Neurobasal-A medium with B-27, 20 μM KCl and NGF 50 ng/ml. AC cultures were maintained as previously described[37]. Cultures were maintained in a humidified incubator with 6.5% CO_2 and fixed with 4% paraformaldehyde after 48 hr.

2.5 Immunostaining

SG, TG, and DRG cultures were immunostained with anti-S100 and anti-neurofilament 200 (NF200) antibodies (1:400, Sigma–Aldrich) to label SCs and neurons, respectively[35]. CGN cultures were immunostained with anti-MAP2 (1:400, Cell Signaling) and anti-TAU1 (1:200, Cell Signaling) antibodies to label dendritic and axonal neurites, respectively. ACs were immunostained with anti-glial fibrillary acidic protein (GFAP) antibody (1:100, Sigma). Alexa 488 and Alexa 546 conjugated secondary antibodies (Invitrogen) were used to detect primary antibody immunolabeling. Slides were cover slipped with ProLong Gold anti-fading reagent with DAPI (Life Technology).

2.6 Determination of Neurite Length and Alignment and Glial Cell Alignment

Digital epifluorescent images were captured on a Leica DMIRE2 microscope (Leica Microsystems, Bannockburn, IL) with Leica DFC350FX digital camera and Metamorph software (Molecular Devices, Silicon Valley, CA). SGN total neurite length was determined from digital images by measuring the longest process of 100 randomly selected neurites from each condition using the measurement tool in Image J (NIH, Bethesda, MD) as previously described[39]. For TG or DRG neurons, total neurite length was determined by averaging the length of six branches of each neuron for 100 neurons at each condition. Neurite alignment was calculated with a modification of our prior method[33]. Briefly, alignment to the pattern was defined as a ratio of unaligned length per neurite length. The ratio is represented as $[(T_L - A_L)/T_L]$, where T_L is total neurite length and A_L represents aligned length in the pattern direction. Aligned length (A_L) was determined by measuring the distance from the neuronal cell body to the neurite terminus in a straight line in the

direction of the micropattern. The pattern direction was always set horizontally prior to measurements. The unaligned length per neurite length ratio is referred to as the alignment ratio throughout the text. A ratio close to zero represents a neurite that closely follows the pattern along its entire length. A wandering neurite, which does not strongly align to the pattern, has a high alignment ratio. To analyze neurite alignment on unpatterned substrates, aligned distance was arbitrarily measured directly along the horizontal plane.

SC and AC orientation was determined as previously described by drawing the outline of the cell using Image J software and fitting an ellipse to the cell outline[33]. The angle made between the major axis of the ellipse and the pattern (θ) was measured in Image J as glial cell alignment.

2.7 Statistics

Statistical analysis was performed using SigmaStat 3.5 software (Systat Software, Chicago, IL). A two-tailed t-test was used to compare cellular alignment between unpatterned and patterned samples followed by a *post hoc* Mann-Whitney Rank Sum Test when normality criteria were not met. Multiple groups were compared by performing a one-way ANOVA followed by a *post hoc* Kruskal-Wallis analysis of variance on ranks and a Dunn's Method multiple comparison procedure. Results were considered statistically significant if $p < 0.05$.

3. Results and discussion

3.1 Micropattern Fabrication

To generate micropatterns suitable for contact guidance studies of inner ear neural elements, Ronchi rule photomasks were used to spatially control the polymerization of a 40 wt% hexyl methacrylate (HMA) and 59 wt% 1,6 – hexanediol dimethacrylate (HDDMA) mixture with 1 wt% 2,2-dimethoxy-2-phenylacetophenone (DMPA) as the photoinitiator (Fig 1). Ronchi rule optics, typically used for optical testing, have alternating transparent (glass) and reflective (chrome) bands of equal size which, during photopolymerization, direct light to areas intended for polymerization and block irradiation at adjacent areas (Fig 1A). Spatially controlling the UV irradiation in this manner varies polymerization speed locally in the substrate and leads to repeating, raised micro-scale physical features useful for cellular contact guidance studies. Ruling band size is used to control micro-feature width and frequency, with mask bands ranging from 5 – 50 μm wide. Periodicity for this study is defined as the distance between two repeating points while tracing a line normal to the bands and ranges from 10 – 100 μm, or double the band width. Fabricating micropatterns using photomasking techniques in conjunction with photopolymerization has also been leveraged for other biomaterial applications. For example, 3D hydrogels have been selectively functionalized with biochemical patterns (i.e. gradients) of defined magnitude and slope by using spatially controlled thiolene photopolymerization[40]. Additionally, tissue engineering constructs have been fabricated with both micro- and macro-porous structure that is spatially tunable through photopolymerization [41]. However, these studies used photomasks and photopolymerization to control chemical composition or structure of 3D matrices rather than to generate surface features for cell contact guidance. Polymer adhesion to glass substrates is facilitated by covalently bonding methacrylated silicon bonding agents to the substrate glass

via silanization[42–44]. Free methacrylate moieties on the surface then form covalent bonds with the newly formed polymer during photopolymerization and prevent delamination events.

During UV exposure, polymerization occurs rapidly under transparent bands that transmit most of the intensity from the light source. In irradiated regions, polymer chain concentration increases while unreacted monomer concentration quickly decreases. Consequently, a local concentration gradient at the interface with masked regions develops for both species. Small molecule monomers diffuse rapidly down the concentration gradient and polymerize in the reactive region exposed to full light intensity. The net positive mass transfer to irradiated regions results in raised, micro-scale surface features. Masked regions still undergo polymerization but do so more slowly than unmasked areas. Polymerization under masked regions principally occurs due to angled diffraction of light as it passes through narrow (micro-scale) slits[45,46], reflections from the glass substrate, and diffusion of propagating polymer chains into shadowed regions. Consequently, light intensity varies under masked regions and generally decreases, which also decreases the polymerization rate, as distance from the original transparent band increases. Larger, propagating polymer chains diffuse more slowly toward masked regions than do unreacted monomers to irradiated areas.

As a result of the masked photopolymerization, a pattern of gradually sloping parallel micro-ridges and grooves of uniform width and amplitude rapidly develop across the entire substrate surface in a single fabrication step. White light interferometry was used to characterize the micropatterns, including measurements of channel amplitude and feature spacing, in both 2D and 3D (Fig 1B). As expected, the distance between repeating points, e.g. a ridge peak to an adjacent ridge peak, closely matches photomask periodicity. Channel amplitudes range from ~250 nm – 10 μm on HMA-co-HDDMA materials polymerized by this method depending on reaction parameters. Any residual monomer under masked regions was removed by an ethanol wash following detachment of the photomask.

Parallel ridges and grooves, or micro-channels, have been used in a wide variety of contact guidance studies, including those used for neurite outgrowth[47–50]. Linear micro-channels are advantageous because they are geometrically simple and facilitate pattern production and characterization as well as analysis of cellular behavior, particularly in the direction of the micro-features. However, the majority of parallel ridge-groove contact guidance studies use various lithographic techniques to fabricate micron and sub-micron features[30,48,51–55]. The resultant pattern features have sharp zero-one transitions with a virtually infinite slope. As a contrast to zero-one features, generating micropatterns by photopolymerizing directly under a photomask leads to smooth, gradually sloping transitions between ridges and grooves.

To demonstrate gradually sloping transitions between ridges and grooves generated via photopolymerization and photomasking, and to confirm interferometric measurements, scanning electron microscopy (SEM) was used to further characterize patterned substrate morphology (Fig 2). Repeating features are seen across the entire substrate surface and vary in frequency based on photomask band spacing (Fig 2A, D). Polymer film thickness is 18 μm and absolute channel amplitude changes as a percentage of the thickness according to

reaction conditions such as photoinitator concentration and UV exposure time. The smooth transitions observed by SEM are likely to more realistically represent physical features of *in vivo* environments compared with sharp or abrupt features, and could be pertinent to contact guidance studies of other neural elements or for different cells (e.g. stem cells). Furthermore, because transitional slope can be adjusted by altering feature frequency or height, cellular behavior that is not apparent on zero-one patterns may be more readily observed and understood. For example, a critical feature slope may induce a desired cellular behavior, such as neurite alignment, gene expression, cell motility, or stem cell differentiation. Additionally, careful tuning of feature slope may facilitate studies aimed at identifying the mechanisms by which cells sense and respond to physical features. Such studies require the ability to inhibit or enhance pattern-induced cellular alignment by manipulating the underlying signaling events. Quantitative changes in alignment are more likely to be apparent on smooth transitions compared with zero-one patterns which have sharp physical features that dominate cellular morphological responses. Such an approach would enable targeted probing of contact guidance mechanisms.

3.2 Tunability of Micropattern Features via Photopolymerization

To investigate the extent of spiral ganglion Schwann cell (SGSC) and spiral ganglion neuron (SGN) neurite alignment to variations in surface topography, microfeature frequency and amplitude were tuned by varying photomask band spacing and by modulating photopolymerization reaction parameters, respectively (Fig 3). Specifically, ridge and groove width, which also dictate pattern periodicity, were controlled by using Ronchi rule photomasks with band spacings of 5 – 50 μm. Faithful reproduction of band spacing was observed for all gratings. However, maximum attainable amplitude becomes more limited at smaller periodicities due to increasing diffraction angles of initiating radiation as band space narrows which increases polymerization in masked regions. Also, smaller reaction volumes beneath narrow high intensity bands decrease mass available for diffusion to reactive areas, and thus limit maximum feature size (Fig 3A). For example, the maximum amplitude attained with a 100 μm periodicity mask is approximately 11 μm compared to about 2 μm using a 10 μm periodicity mask. Furthermore, channel amplitude is generally lower at any given time increment for patterns polymerized under photomasks with smaller periodicities (i.e. more frequent bands). Therefore, to enable meaningful neurite alignment for comparison across multiple feature spacings, only periodicities of 10 μm or higher were used for cell studies.

Micro-channel amplitude for the HMA-co-HDDMA system can be varied by almost two orders of magnitude (from 250 nm – 10 μm) through modulation of reaction parameters of the polymerization reaction (results are only shown for the 1 – 10 μm regime). Amplitudes smaller than 1 μm are readily generated with 10 μm periodicity masks but are not achieved even at long exposure times with masks that have a 50 μm periodicity or higher. However, generating sub-micron amplitudes for patterns with higher periodicities is achieved by increasing the spacing between the pre-polymer solution and the photomask (data not shown).

To demonstrate the effect of UV exposure time on channel amplitude, pattern samples were cured at controlled time increments (Fig 3). Temporal control of the polymerization is achieved by shuttering the initiating light source at specific time steps, which prevents further initiation events and leads to rapid termination of propagating kinetic chains and, hence, a termination of the polymerization reaction. Temporal control is crucial to pattern formation because it enables arrest of specific micropattern feature sizes as the reaction progresses. Channel amplitude steadily increases to a maximum amplitude as unreacted monomer continues to diffuse into irradiated regions with high reaction rates. At some point during the polymerization, grooves begin to backfill due to polymerization in masked regions. Continued irradiation subsequently leads to smaller and smaller amplitudes until a final amplitude is reached that is approximately 10% of the maximum amplitude. The final pattern is set as diffusion becomes significantly limited due to the vitrification of the polymer and the gelling effect of crosslinked networks. UV exposure time strongly correlates to channel amplitude under the described parameters (Fig 3). Patterned samples were either tacky or exhibited insufficient mechanical strength for characterization and cellular experiments if polymer conversion was too low, i.e. less than 40 s exposure under the given conditions. The correlation between UV exposure time and final feature size demonstrates how quickly and readily multiple sizes, and subsequently slopes, of micro-features can be generated via this facile photopolymerization method.

Modulation of initiating light intensity also serves as a method to control channel amplitude as well as to shift amplitude profiles to different UV exposure times due to changes in reaction rate (Fig 3B). For example, an increase in light intensity raises polymerization reaction rate and shifts final amplitude profiles to earlier polymerization times. At the highest intensity, 80 mW/cm^2, the maximum average amplitude decreases to approximately 7 μm compared to 8 μm when cured at a lower intensity of 8 mW/cm^2. This decrease suggests that polymer gelation or vitrification may inhibit feature size at high reaction rates. Maximum attainable amplitude occurs at an exposure time of 60 s while curing with an 80 mW/cm^2 light intensity which is 30 s faster than the UV exposure time required to reach maximum amplitude with an 8 mW/cm^2 light intensity.

To illustrate the effect of photoinitiator concentration on final channel amplitude, pre-polymer formulations were mixed with 0.1, 1, and 5 wt% DMPA with corresponding reductions in both HMA and HDDMA wt% (Figure 3C). Similar to changes in light intensity, altering polymerization speed by modulating photoinitiator concentration also enables tuning of feature amplitude. For example, maximum average channel amplitude increases by 30% from 8 μm at 1 wt% photoinitiator to 11 μm at 0.1 wt% photoinitiator. While maximum amplitude increases with low photoinitiator concentration, exposure time to reach a maximum increases by 180% as concentration decreases from 5 wt% to 0.1 wt%. The final channel amplitude at long exposure times is also lower for high DMPA concentrations at approximately 0.9 μm and 2 μm for 5wt% and 0.1 wt%, respectively. Furthermore, the entire amplitude profile broadens to larger time increments at low DMPA concentration. Similar broadening of the amplitude profile occurs while using a low (8 mW/cm^2) irradiation intensity. Increases in feature amplitude at low photoinitiator concentrations support the observation that speed of reaction should be considered when targeting a specific feature size due to gelation constraints. Decreases in channel amplitude

at UV exposure times above the maximum amplitude time step are likely caused by backfilling of masked regions. Continued diffusion of propagating species as well as generation of new active centers by diffracted as well as internally reflected light may enable masked or groove regions to polymerize, thus, resulting in a decrease of the final measured amplitude. Even with these differences, final channel amplitude is still about 10% of the maximum channel amplitude at high light intensity and long curing times (> 500 s).

3.3 Alignment of Multiple Neural and Glial Cell Types to Sloping Micropatterns

Our labs have previously demonstrated robust growth of SGNs on unpatterned, as well as some alignment on patterned, HMA-co-HDDMA polymers similar to those used for this study[33]. However, to determine if gradually sloping micro-channels induce general sensory neurite alignment, alternative sensory neuronal populations were cultured on patterned polymers as well as on unpatterned controls (Fig 4). Specifically, SGN neurite alignment was compared to DRGN and TGN neurite alignment, which are also sensory neurons of the peripheral nervous system (PNS). Each neuronal population was cultured on a micropattern with a periodicity of 50 μm and channel amplitude of 3 μm.

As seen in Figure 4, *de novo* neurite growth for each sensory neuronal type extends randomly on unpatterned HMA-co-HDDMA and is analogous to neuritic process growth on laminin coated glass[39]. Conversely, gradually sloping microchannels formed by the described photopolymerization method induce general neurite alignment among each neuronal population. SGN neurites strongly align to the pattern along the majority of their path length. SGNs show a typical monopolar or bipolar morphology in culture (i.e. one to two primary neurites). DRGNs and TGNs extend multiple primary neuritic processes which is also typical of their standard morphology. While neuritic processes from DRGNs and TGNs align to the micropattern, they do not align as strongly along the entire process length compared with SGN neurites. DRGN and TGN neurites initially extend radially from the soma on patterned substrates with apparently little sensitivity to the pattern direction. However, given sufficient distance, the majority of primary neurites turn and align to the pattern direction along the terminal portion of the neurite.

To quantitatively evaluate sensory neurite response to micropatterns, alignment was measured on unpatterned and patterned substrates using the previously described alignment ratio (Fig 5). Differences between neuritic process alignment on unpatterned compared to patterned samples are significant for each sensory neuronal population. As observed from epifluorescent digital images, SGN neurites align more strongly to patterned substrates than neurites from DRGNs and TGNs. SGN neurites exhibited less than half of the unaligned length per length of neurite shown by the other sensory neurites. The alignment ratios of each type of sensory neurite on unpatterned substrates are not statistically different. Neurite alignment from cerebellar granular neurons (CGN), which are part of the central nervous system (CNS), was also evaluated. CGN MAP 2-positive dendritic neurites align to patterned substrates and show random growth on unpatterned surfaces (Fig 5B). However, CGN Tau-positive axonal neurites do not significantly align to micropatterns of the given dimensions. While regenerative neurites from various neuronal types align to microfeatures,

differences in neurite alignment indicate that specific neural populations, and even neural process types, respond to physical cues to varying degrees.

Having previously demonstrated basic SGSC alignment on micropatterned HMA-co-HDDMA polymers[33], astroycytes (ACs) from the CNS were cultured on unpatterned and patterned polymers as a glial cell alternative to determine if similar micro-features induce general glial cell alignment (Fig 6). AC cultures were prepared from P5 rat cerebral cortex and were plated on substrates coated with poly-lysine. ACs demonstrate typical morphology on unpatterned substrates. By contrast, ACs elongate and align in the direction of micro-channels on patterned samples with the same dimensions (50 μm periodicity and 3 μm amplitude) used for neuronal studies. As described previously, SGSC and AC alignment to pattern features was evaluated by measuring the angle between the major axis of a cell outline and the pattern direction (horizontal) [33]. Glial cells that made an angle of 10° or less with the pattern are considered aligned. The mean ellipse angle of ACs cultured on unpatterned polymers is almost three times the mean angle on patterned samples. As a population, 55% of ACs align (i.e. 10° or less) to microfeatures (Fig 6D) with a 50 μm periodicity and 3 μm amplitude, which is even greater than the 40% of SGSCs that align to similar features (Fig 7F). Interestingly, while ACs and SGSCs align to the described features, fibroblasts do not strongly align to features on a similar size scale[33].

3.4 Extent of SGN Neurite and SGSC Alignment based on Feature Dimensions

Pattern shapes ultimately dictate the final direction taken by SGN neurites or SGSCs that orient to the micro-features. However, to evaluate the influence of channel amplitude on the extent of SGN neurite and SGSC alignment, the cells were cultured on micropatterns with varied amplitude but constant periodicity (Fig 7). Specifically, SGSCs and dissociated SGNs were cultured on patterns with a constant periodicity of 50 μm but with varying channel amplitudes of 1.0±0.1, 3.1±0.3, and 8.1±0.8 μm, which will be referred to as 1, 3, and 8 μm, respectively. To tune channel amplitude, the irradiation source was shuttered at specific time intervals to temporally arrest the polymerization during pattern development. SGN neurite length does not appear to change with different amplitudes. In addition to maintaining similar average lengths, the spread of neurite lengths for SGNs cultured on patterned substrates shows no observable effect of channel amplitude on absolute length (Fig 7B).

Conversely, SGN neurite alignment increases significantly with increasing channel depth. SGN neurites have a low average alignment ratio of 0.045 on 8 μm deep channels, which is approximately three times more aligned than neurites on 1 and 3 μm amplitude samples with ratios of 0.16 and 0.13, respectively (Fig 7C). The low alignment ratio on 8 μm amplitude channels also indicates that the neurites strongly align to the pattern along their entire path length. Alignment along the length of a neurite may be crucial to preserve signal fidelity by limiting interaction with adjacent neurites since unaligned regions of a neurite are more likely to encounter and interact with other neurites. Furthermore, to limit inaccurate spatial signaling, it may be necessary to maintain tight control over a population of tens to thousands of neurites within a specific region. It is therefore important to note that greater than 90% of the SGN population cultured on the 8 μm deep channels exhibit alignment ratios of 0.10 or lower while 100% of the neurites produce alignment ratios less than 0.25.

Approximately 60% of neurites on 1 μm and 70% on 3 μm channels align fairly well to the pattern with a ratio of 0.15 or lower, however, a significant percentage remains with ratios higher than 0.30 (Fig 7D). While wandering neurites may align to the pattern throughout some of their length, a significant portion may not track in the pattern direction which could ultimately lead to a loss of stimulatory specificity and resolution. Accordingly, microtopography fabricated for neurite alignment should be designed to quickly orient and maintain spatial control of neuritic processes along their entire length.

Along with SGN neurite contact guidance, it may also be advantageous to develop an understanding of SGSC response to cell relevant physical features due to their close association with SGNs and their processes[33,56,57]. For example, SGSCs closely associate with regenerative neurites *in vitro* and express neurotrophins such as BDNF and NT-3 that provide crucial trophic support to maintain SGN viability and support neurite growth[35,56,57]. Accordingly, the extent of SGSC alignment in response to patterns with constant periodicity but varied feature amplitude was evaluated by co-culturing SGSCs with SGNs on micropatterned HMA-co-HDDMA polymers with 1, 3, and 8 μm channel amplitudes and 50 μm periodicity (Fig 7E,F). SGSC alignment was quantified by the same method used for AC alignment. Similar to SGN neurite alignment, SGSC alignment to parallel line-space gratings with gradual slopes also significantly increases with increasing channel amplitude (Fig 7E). Taken as a population, the percentage of SGSCs that align within 10° to the pattern direction is 25%, 40%, and 70% for 1, 3, and 8 μm channels, respectively.

To determine if the change in neurite alignment in response to channel depth was specific to SGN neurites, DRGN neurite alignment was also evaluated on patterns with increasing micro-channel amplitude (Fig 8). It was previously noted that DRGN neurites had two times as much unaligned length per length of neurite compared to SGN neurites on patterns with a 50 μm periodicity and a 3 μm depth. However, on patterns with an 8 μm channel amplitude and 50 μm periodicity, DRGN neurite alignment (ratio of 0.054) is not significantly different from SGN neurite alignment (ratio of 0.045) on the same features (Fig 8A). Additionally, DRGN neurites branch extensively as well as cross over pattern features several times at the proximal end of the neurite (i.e. near the soma) on patterns with a 50 μm periodicity and a 3 μm amplitude. However, DRGN primary neurites and their branches appear to be maintained within micropattern features due to strong alignment effects from physical surface cues on patterns with the same periodicity but deeper channels (8 μm). Therefore, while different neurons may respond to physical guidance cues to varying degrees at one size scale, they appear to exhibit similar guidance behavior after reaching a critical feature slope or amplitude.

To determine the effect of feature frequency, or periodicity, on the extent of neural process alignment, SGN neurite alignment was measured on patterns with a constant amplitude of 1 μm but with periodicities of 10, 33.3, and 50 μm (Fig 9). Micropattern periodicity is controlled using Ronchi rule photomasks with various band spacings, while consistent amplitude for various periodicities is achieved by controlling UV exposure time. SGN neurites are three times more aligned on patterns with a 10 μm periodicity compared to patterns with 50 μm periodicities (Fig 9A). Interestingly, SGN neurite alignment on a 10 μm

periodicity and relatively shallow 1 μm amplitude pattern is not statistically different than their alignment on a 50 μm periodicity and 8 μm deep amplitude pattern. Additionally, over 95% of the population of SGN neurites cultured on patterns with a 10 μm periodicity but shallow amplitude of 1 μm fall below the low alignment ratio of 0.10 (Fig 9B). While approximately 60% of neurites on patterns with a 33.3 μm periodicity and 50% of neurites on patterns with a 50 μm periodicity also fall below a ratio of 0.10, there still remains a large percentage of the population that weakly aligns. The strong alignment observed on 1 μm amplitude samples with frequent features may be due to several contributing factors. Specifically, patterns that have smaller periodicities present more opportunities for a regenerative neuritic process to encounter a physical feature and orient to the pattern direction over a given distance than those with larger periodicities. Moreover, decreasing pattern periodicity while maintaining channel amplitude increases the slope between minimum groove depths and the adjacent maximum ridge heights. Photopolymerization of micropattered topography is, therefore, a useful and facile method to determine cellular response to feature slope and spacing.

3.5 SGN Neurite Alignment on Nano-Scale Features

Having determined that SGN neurites strongly align to shallow (1 μm) but frequent (10 μm) features, we next sought to determine the extent to which SGN neurites align to nano-scale (< 1 μm) and frequent features (Fig 10). Nano-scale features are fabricated by curing samples with long UV exposure times (> 100 s) under 10 μm periodicity masks. Narrower bands increase the angle of diffracted light and, therefore, increase polymerization under masked regions, leading to greater backfilling and shallower features. Narrow band spacing also decreases reaction volume of each irradiated region which allows for less mass transfer for producing raised regions. Uniform and reproducible amplitudes of approximately 250 nm and 500 nm were generated using UV exposure increments of 300 s and 125 s, respectively. SEM confirms that overall polymer thickness remained constant (~18 μm) and that the pattern depth is only a small fraction of the film thickness from vertical examination based on cross-sectional imaging (Fig 10A, B). SGN neurites strongly align to patterns with channel amplitudes of 250 nm and 500 nm and show random growth on unpatterned controls (Fig 10). Interestingly, SGN neurite alignment on 250 nm amplitude channels with a 10 μm periodicity was not statistically different from alignment on 8 μm amplitude channels with a 50 μm periodicity. As indicated by their low alignment ratio, regenerative SGN neurites on 250 nm deep channels align along their entire path length which is similar to SGN neurite alignment on channels with an 8 μm amplitude and 50 μm periodicity (Fig 10C, D).

Other neuritic processes, namely those from sympathetic and DRG neurons, also align to nano-scale line-space gratings (depth 300 nm, width 100 – 400 nm)[15]. However, the vertical slopes inherent to lithographic techniques contrast with the sloped transitions between ridges and grooves developed by photopolymerization in this study. In either case, both for SGNs and sympathetic neurons, neuritic growth cones that are several microns in diameter are sensitive enough to respond and align to features that are smaller by an order of magnitude. Accordingly, it is evident that nano-scale features should be considered for alignment of neurites for both *in vitro* contact guidance studies as well as for future

applications intended to improve neural-implant interfaces by spatial organization of sensory elements.

3.6 Correlation of Maximum Feature Slope with SGN Neurite Alignment

SGN neurite alignment improves as amplitude increases with constant periodicity and also improves as periodicity decreases with constant amplitude. In both cases, the slope grade that transitions between grooves and ridges also increases. Accordingly, to determine if changes in neurite alignment correlate to feature slope, AFM was used to quantify the average and maximum slope that occur between groove minimums and adjacent ridge maximums of each pattern used for neurite contact guidance. As indicated in Table 1, average and maximum slope increase as channel amplitude increases for a given periodicity and neurite alignment correspondingly increases. Figure 11 illustrates the correlation between neurite alignment and average feature slope as well as neurite alignment and maximum feature slope on a linear regression plot. Average slope between ridge-groove transitions moderately correlates with SGN alignment ($r=0.67$) but is not considered significant ($p > 0.05$). However, maximum slope strongly correlates with neurite alignment ($r=0.93$) and is significant ($p < 0.005$). In fact, slope appears to be a much stronger predictor of alignment than either periodicity or amplitude. Interestingly, an average diameter of an SGN growth cone is approximately 5 μm but features as small as 250 nm cause significant neurite contact guidance when maximum feature slope is sufficiently steep. Therefore, neurite alignment and subsequent spatial control by physical cues may depend more strongly on feature contrast than on absolute feature height.

4. Conclusion

Spatially directing regenerative sensory neurites to stimulative prostheses elements may serve as a viable method to improve neural prosthetic performance including enhanced tonal resolution for cochlear implants. Accordingly, in this study we describe a facile photopolymerization method to fabricate tunable methacrylate micropatterns that align inner ear neural elements, namely, regenerative spiral ganglion neuron (SGN) neurites and spiral ganglion Schwann cells (SGSCs), based on physical surface cues. Gradually sloping micro- and nano-scale features generated by this method were tuned to investigate the extent of SGN neurite alignment in response to modulations in feature amplitude, frequency, and slope. Channel amplitude can be controlled from 250 nm – 10 μm by modulating UV exposure time, initiating light intensity, and photoinitiator concentration, while pattern periodicity is regulated by grating dimensions. Glial cells as well as neurites from SGNs, DRGNs, TGNs, and CGNs align to the photopolymerized micropatterns, but alignment varies among cell types. Alignment of neural elements increases significantly with increasing feature amplitude as well as with decreasing periodicity. SGN neurites, which are typically several microns in diameter, also strongly align to patterns with nano-scale (250 and 500 nm) channel amplitudes and more frequent features. Furthermore, SGN neurite alignment strongly correlates ($r=0.93$) with maximum feature slope, which can tuned by feature amplitude and periodicity. This photopolymerization fabrication method serves as an additional surface engineering tool that enables investigation of cell-material interactions in response to slope of micron and sub-micron scale features. The research also informs efforts

to direct nerve growth for improved performance of neural prosthetics that currently provide low stimulatory specificity due to spatial resolution challenges.

Acknowledgments

The authors acknowledge funding support from the National Science Foundation (CBET-0933450), the National Institutes of Health (NCRR-UL1RR024979 and NIDCD-P30 DC010362), and the American Hearing Research Foundation. We also acknowledge government support from the Department of Defense, Air Force Office of Scientific Research, for a National Defense Science and Engineering Graduate (NDSEG) Fellowship, 32 CFR 168a. We also thank Brian Dillman for his help with acquisition of detailed slope information via AFM. The work was facilitated by the Microfabrication Laboratory and Central Microscopy core facilities at the University of Iowa.

References

1. Leach JB, Achyuta AK, Murthy SK. Bridging the Divide between Neuroprosthetic Design, Tissue Engineering and Neurobiology. Front Neuroeng. 2010; 2:18. [PubMed: 20161810]
2. O'Leary SJ, Richardson RR, McDermott HJ. Principles of design and biological approaches for improving the selectivity of cochlear implant electrodes. Journal of Neural Engineering. 2009; 6:055002. [PubMed: 19721188]
3. Winter JO, Cogan SF, Rizzo JF III. Retinal prostheses: current challenges and future outlook. Journal of Biomaterials Science-Polymer Edition. 2007; 18:1031–1055. [PubMed: 17705997]
4. Rubinstein JT. How cochlear implants encode speech. Curr Opin Otolaryngol Head Neck Surg. 2004; 12:444–8. [PubMed: 15377959]
5. Shannon RV, Fu QJ, Galvin J 3rd. The number of spectral channels required for speech recognition depends on the difficulty of the listening situation. Acta Otolaryngol Suppl. 2004; (552):50–54. [PubMed: 15219048]
6. Brors D, Aletsee C, Schwager K, Mlynski R, Hansen S, Schäfers M, Ryan AF, Dazert S. Interaction of spiral ganglion neuron processes with alloplastic materials in vitro. Hear Res. 2002; 167:110–121. [PubMed: 12117535]
7. Evans AJ, Thompson BC, Wallace GG, Millard R, O'Leary SJ, Clark GM, Shepherd RK, Richardson RT. Promoting neurite outgrowth from spiral ganglion neuron explants using polypyrrole/BDNF-coated electrodes. Journal of Biomedical Materials Research Part a. 2009; 91A: 241–250. [PubMed: 18814235]
8. Roehm PC, Hansen MR. Strategies to preserve or regenerate spiral ganglion neurons. Curr Opin Otolaryngol Head Neck Surg. 2005; 13:294–300. [PubMed: 16160524]
9. Leng T, Wu P, Mehenti NZ, Bent SF, Marmor MF, Blumenkranz MS, Fishman HA. Directed retinal nerve cell growth for use in a retinal prosthesis interface. Invest Ophthalmol Vis Sci. 2004; 45:4132–4137. [PubMed: 15505066]
10. Mehenti NZ, Peterman MC, Leng T, Marmor MF, Blumenkranz MS, Bent SF. A retinal interface based on neurite micropatterning for single cell stimulation. Invest Ophthalmol Vis Sci. 2003; 44:U704–U704.
11. Guenther E, Troger B, Schlosshauer B, Zrenner E. Long-term survival of retinal cell cultures on retinal implant materials. Vision Res. 1999; 39:3988–3994. [PubMed: 10748931]
12. Cui XY, Wiler J, Dzaman M, Altschuler RA, Martin DC. In vivo studies of polypyrrole/peptide coated neural probes. Biomaterials. 2003; 24:777–787. [PubMed: 12485796]
13. Hurtado A, Cregg JM, Wang HB, Wendell DF, Oudega M, Gilbert RJ, McDonald JW. Robust CNS regeneration after complete spinal cord transection using aligned poly-L-lactic acid microfibers. Biomaterials. 2011; 32:6068–6079. [PubMed: 21636129]
14. Miller C, Jeftinija S, Mallapragada S. Synergistic effects of physical and chemical guidance cues on neurite alignment and outgrowth on biodegradable polymer substrates. Tissue Eng. 2002; 8:367–378. [PubMed: 12167224]
15. Johansson F, Carlberg P, Danielsen N, Montelius L, Kanje M. Axonal outgrowth on nano-imprinted patterns. Biomaterials. 2006; 27:1251–1258. [PubMed: 16143385]

16. Wangensteen KJ, Kalliainen LK. Collagen Tube Conduits in Peripheral Nerve Repair: A Retrospective Analysis. Hand (N Y). 2009
17. Richardson JA, Rementer CW, Bruder JM, Hoffman-Kim D. Guidance of dorsal root ganglion neurites and Schwann cells by isolated Schwann cell topography on poly(dimethyl siloxane) conduits and films. Journal of Neural Engineering. 2011; 8:046015. [PubMed: 21673394]
18. Schmalenberg KE, Uhrich KE. Micropatterned polymer substrates control alignment of proliferating Schwann cells to direct neuronal regeneration. Biomaterials. 2005; 26:1423–1430. [PubMed: 15482830]
19. Branch DW, Wheeler BC, Brewer GJ, Leckband DE. Long-term stability of grafted polyethylene glycol surfaces for use with microstamped substrates in neuronal cell culture. Biomaterials. 2001; 22:1035–1047. [PubMed: 11352085]
20. Gustavsson P, Johansson F, Kanje M, Wallman L, Linsmeier CE. Neurite guidance on protein micropatterns generated by a piezoelectric microdispenser. Biomaterials. 2007; 28:1141–1151. [PubMed: 17109955]
21. Oliva AA, James CD, Kingman CE, Craighead HG, Banker GA. Patterning axonal guidance molecules using a novel strategy for microcontact printing. Neurochem Res. 2003; 28:1639–1648. [PubMed: 14584818]
22. Wittig JH, Ryan AF, Asbeck PM. A reusable microfluldic plate with alternate-choice architecture for assessing growth preference in tissue culture. J Neurosci Methods. 2005; 144:79–89. [PubMed: 15848242]
23. Li S, Li H, Wang Z. Orientation of spiral ganglion neurite extension in electrical fields of charge-balanced biphasic pulses and direct current in vitro. Hear Res. 2010; 267:111–118. [PubMed: 20430073]
24. Yao L, Pandit A, Yao S, McCaig CD. Electric Field-Guided Neuron Migration: A Novel Approach in Neurogenesis. Tissue Engineering Part B-Reviews. 2011; 17:143–153. [PubMed: 21275787]
25. Teixeira AI, Abrams GA, Bertics PJ, Murphy CJ, Nealey PF. Epithelial contact guidance on well-defined micro- and nanostructured substrates. J Cell Sci. 2003; 116:1881–1892. [PubMed: 12692189]
26. Chou L, Firth J, Uitto V, Brunette D. Substratum surface topography alters cell shape and regulates fibronectin mRNA level, mRNA stability, secretion and assembly in human fibroblasts. J Cell Sci. 1995; 108:1563–1573. [PubMed: 7615675]
27. Dalby MJ, Gadegaard N, Tare R, Andar A, Riehle MO, Herzyk P, Wilkinson CDW, Oreffo ROC. The control of human mesenchymal cell differentiation using nanoscale symmetry and disorder RID E-9243-2010 RID A-3427-2011. Nature Materials. 2007; 6:997–1003.
28. Anselme K, Bigerelle M, Noel B, Dufresne E, Judas D, Iost A, Hardouin P. Qualitative and quantitative study of human osteoblast adhesion on materials with various surface roughnesses RID D-8909-2011. J Biomed Mater Res. 2000; 49:155–166. [PubMed: 10571901]
29. Spivey EC, Khaing ZZ, Shear JB, Schmidt CE. The fundamental role of subcellular topography in peripheral nerve repair therapies. Biomaterials. 2012; 33:4264–4276. [PubMed: 22425024]
30. Hsu S, Lu PS, Ni H, Su C. Fabrication and evaluation of microgrooved polymers as peripheral nerve conduits. Biomed Microdevices. 2007; 9:665–674. [PubMed: 17562182]
31. Song M, Uhrich KE. Optimal micropattern dimensions enhance neurite outgrowth rates, lengths, and orientations. Ann Biomed Eng. 2007; 35:1812–1820. [PubMed: 17616821]
32. Rajnicek AM, Britland S, McCaig CD. Contact guidance of CNS neurites on grooved quartz: influence of groove dimensions, neuronal age and cell type. J Cell Sci. 1997; 110:2905–2913. [PubMed: 9359873]
33. Clarke JC, Tuft BW, Clinger JD, Levine R, Figueroa LS, Allan Guymon C, Hansen MR. Micropatterned methacrylate polymers direct spiral ganglion neurite and Schwann cell growth. Hear Res. 2011; 278:96–105. [PubMed: 21616131]
34. Jeon S, Menard E, Park J, Maria J, Meitl M, Zaumseil J, Rogers J? Three-Dimensional Nanofabrication with Rubber Stamps and Conformable Photomasks. Adv Mater. 2004; 16:1369–1373.

35. Hansen MR, Vijapurkar U, Koland JG, Green SH. Reciprocal signaling between spiral ganglion neurons and Schwann cells involves neuregulin and neurotrophins. Hear Res. 2001; 161:87–98. [PubMed: 11744285]
36. Hegarty J, Kay A, Green S. Trophic support of cultured spiral ganglion neurons by depolarization exceeds and is additive with that by neurotrophins or cAMP and requires elevation of [Ca2+](i) within a set range. Journal of Neuroscience. 1997; 17:1959–1970. [PubMed: 9045725]
37. Jeon E, Xu N, Xu L, Hansen MR. Influence of central glia on spiral ganglion neuron neurite growth. Neuroscience. 2011; 177:321–334. [PubMed: 21241783]
38. McCarthy K, Devellis J. Preparation of Separate Astroglial and Oligodendroglial Cell-Cultures from Rat Cerebral Tissue. J Cell Biol. 1980; 85:890–902. [PubMed: 6248568]
39. Roehm PC, Xu N, Woodson EA, Green SH, Hansen MR. Membrane depolarization inhibits spiral ganglion neurite growth via activation of multiple types of voltage sensitive calcium channels and calpain. Molecular and Cellular Neuroscience. 2008; 37:376–387. [PubMed: 18055215]
40. DeForest CA, Sims EA, Anseth KS. Peptide-Functionalized Click Hydrogels with Independently Tunable Mechanics and Chemical Functionality for 3D Cell Culture. Chemistry of Materials. 2010; 22:4783–4790. [PubMed: 20842213]
41. Bryant SJ, Cuy JL, Hauch KD, Ratner BD. Photo-patterning of porous hydrogels for tissue engineering. Biomaterials. 2007; 28:2978–2986. [PubMed: 17397918]
42. Sterman S, Marsden JG. Silane Coupling Agents. Industrial and Engineering Chemistry. 1966; 58:33.
43. Walba DM, Liberko CA, Korblova E, Farrow M, Furtak TE, Chow BC, Schwartz DK, Freeman AS, Douglas K, Williams SD, Klittnick AF, Clark NA. Self-assembled monolayers for liquid crystal alignment: simple preparation on glass using alkyltrialkoxysilanes. Liquid Crystals. 2004; 31:481–489.
44. Weetall HH. Preparation of Immobilized Proteins Covalently Coupled through Silane Coupling Agents to Inorganic Supports. Appl Biochem Biotechnol. 1993; 41:157–188. [PubMed: 8379662]
45. Abbe E. Contributions to the theory of the microscope and the microscopic perception (translated from German). Arch Mikr Anat. 1873; 9:413–468.
46. Garini Y, Vermolen BJ, Young IT. From micro to nano: recent advances in high-resolution microscopy. Curr Opin Biotechnol. 2005; 16:3–12. [PubMed: 15722009]
47. Liliensiek SJ, Wood JA, Yong J, Auerbach R, Nealey PF, Murphy CJ. Modulation of human vascular endothelial cell behaviors by nanotopographic cues. Biomaterials. 2010; 31:5418–5426. [PubMed: 20400175]
48. Mattotti M, Alvarez Z, Ortega JA, Planell JA, Engel E, Alcántara S. Inducing functional radial glia-like progenitors from cortical astrocyte cultures using micropatterned PMMA. Biomaterials. 2012; 33:1759–1770. [PubMed: 22136716]
49. Hsu SH, Chen CY, Lu PS, Lai CS, Chen CJ. Oriented Schwann cell growth on microgrooved surfaces. Biotechnol Bioeng. 2005; 92:579–588. [PubMed: 16261633]
50. Yao L, Wang S, Cui W, Sherlock R, O'Connell C, Damodaran G, Gorman A, Windebank A, Pandit A. Effect of functionalized micropatterned PLGA on guided neurite growth. Acta Biomaterialia. 2009; 5:580–588. [PubMed: 18835227]
51. Gasiorowski JZ, Liliensiek SJ, Russell P, Stephan DA, Nealey PF, Murphy CJ. Alterations in gene expression of human vascular endothelial cells associated with nanotopographic cues. Biomaterials. 2010; 31:8882–8888. [PubMed: 20832112]
52. Ferrari A, Cecchini M, Serresi M, Faraci P, Pisignano D, Beltram F. Neuronal polarity selection by topography-induced focal adhesion control. Biomaterials. 2010; 31:4682–4694. [PubMed: 20304485]
53. Miyoshi H, Adachi T, Ju J, Lee SM, Cho DJ, Ko JS, Uchida G, Yamagata Y. Characteristics of motility-based filtering of adherent cells on microgrooved surfaces. Biomaterials. 2012; 33:395–401. [PubMed: 22019118]
54. Charest J, Eliason M, Garcia A, King W. Combined microscale mechanical topography and chemical patterns on polymer cell culture substrates. Biomaterials. 2006; 27:2487–2494. [PubMed: 16325902]

55. Francisco H, Yellen BB, Halverson DS, Friedman G, Gallo G. Regulation of axon guidance and extension by three-dimensional constraints. Biomaterials. 2007; 28:3398–3407. [PubMed: 17467794]

56. Bostrom M, Khalifa S, Bostrom H, Liu W, Friberg U, Rask-Andersen H. Effects of Neurotrophic Factors on Growth and Glial Cell Alignment of Cultured Adult Spiral Ganglion Cells. Audiology and Neuro-Otology. 2010; 15:175–186. [PubMed: 19851064]

57. Whitilon DS, Tieu D, Grover M, Reilly B, Coulson MT. Spontaneous Association of Glial Cells with Regrowing Neurites in Mixed Cultures of Dissociated Spiral Ganglia. Neuroscience. 2009; 161:227–235. [PubMed: 19324078]

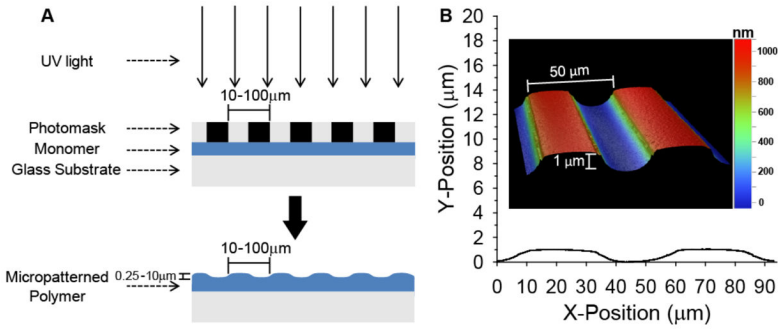

Figure 1.

Schematic of photopatterning process. **A)** Photopolymerizable monomer is selectively exposed to UV light through a photomask resulting in raised microfeatures across the surface. **B)** A 2D profile is shown of a micropatterned HMA-co-HDDMA substrate with a 50 μm periodicity and a channel amplitude of 1 μm. Inset: 3D representation of a 100 μm^2 area as measured by white light interferometry.

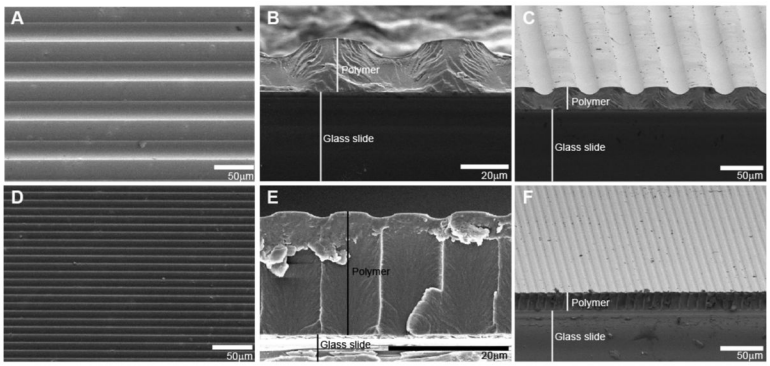

Figure 2.

Representative SEM images of micropatterned HMA-co-HDDMA polymers. **A–C)** SEM images of a pattern with 50 μm periodicity and channel amplitude of 8 μm. **D–F)** SEM images of a pattern with 10 μm periodicity and channel amplitude of 1 μm. Shown are: top down views (A),(D); cross-sectional views (B),(E); and angled cross-sectional views (C), (F). Gradual transitions between ridges and grooves are evident in photopolymerized micropatterns.

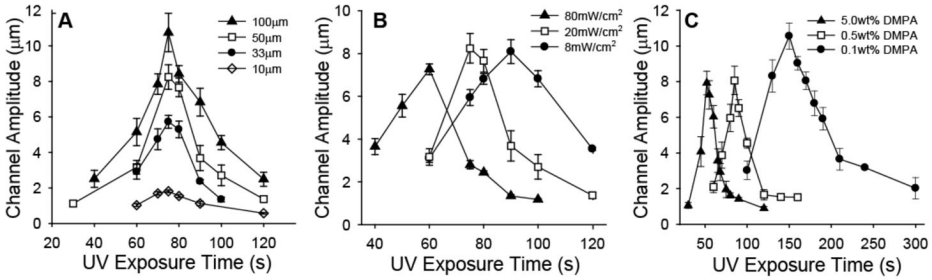

Figure 3.

Tuning of micropattern features by variations in photomask band sizing, light intensity, photoinitiator concentration, and UV exposure time. **A)** Feature frequency is controlled by photomask design. Amplitude profiles represent photomasks with periodicities of 100, 50, 33, and 10 μm. Maximum attainable amplitude is limited as periodicity (mask band size) decreases. **B)** Channel amplitude as a function of varying initiating light intensity and UV exposure time. **C)** Channel amplitude as a function of photoinitiator concentration as well as UV exposure time. Periodicity for all trials in (B) and (C) is 50 μm. Each point indicates mean±SD.

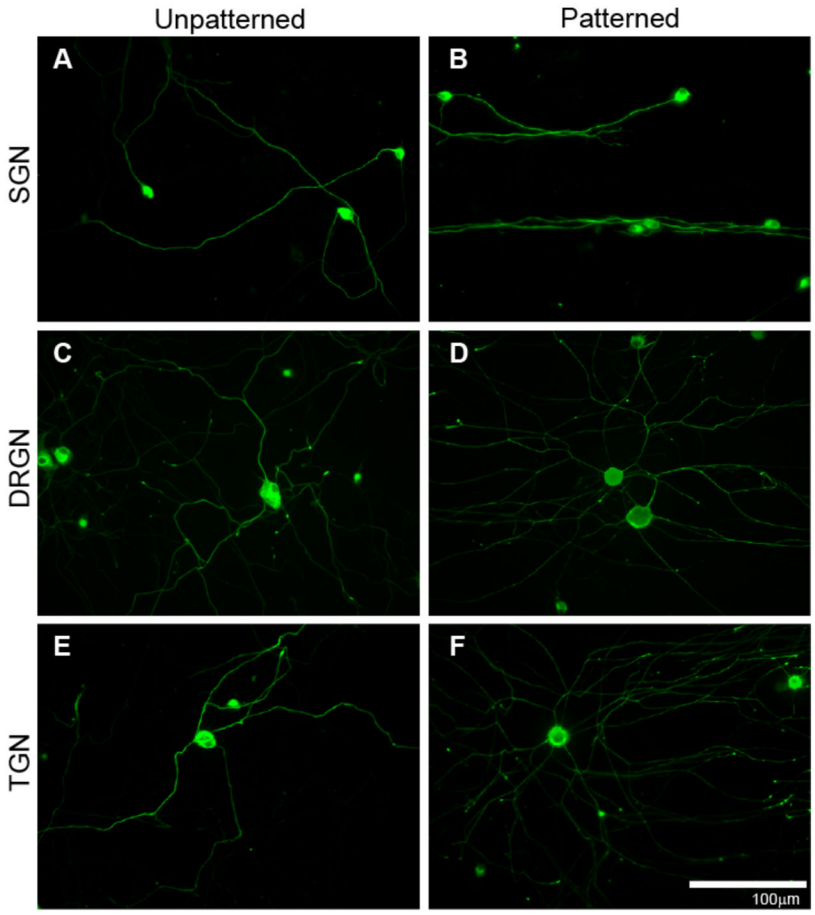

Figure 4.

Neurite growth from dissociated SGNs (A),(B), DRGNs (C),(D), and TGNs (E),(F) on unpatterned (left column) and patterned (right column) HMA-co-HDDMA polymers. Neurite growth extends randomly on unpatterned substrates but aligns to topographic features on patterned substrates. Cultures were stained with anti-NF200 antibodies. Micropatterned substrates have periodicities of 50 μm and channel amplitudes of 3 μm. The pattern is oriented horizontally.

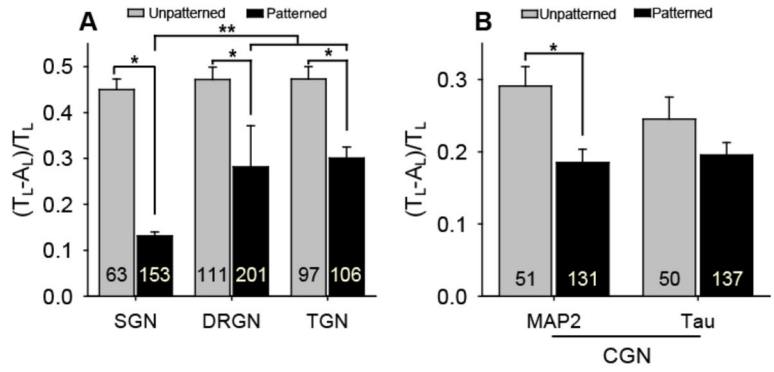

Figure 5.

Unaligned length per neurite length ratios (mean±SE) for multiple neuronal types cultured on unpatterned and patterned substrates. **A)** Neurite alignment from dissociated SGNs, DRGNs, and TGNs is statistically different on patterned substrates compared to unpatterned controls (*$p < 0.005$, Mann-Whitney Rank Sum test). SGN neurites align more strongly to the pattern than DRGN and TGN neurites (**$p < 0.001$, one way ANOVA). **B)** Dendritic neurite (MAP 2-positive) alignment from dissociated CGNs is statistically different on patterned substrates compared to an unpatterned control (*$p < 0.005$, Mann-Whitney Rank Sum test). However, axonal neurite (Tau-positive) alignment from dissociated CGNs is not statistically different ($p = 0.135$) from an unpatterned control. Micropatterns used for each neuronal culture have periodicities of 50 μm and channel amplitudes of 3 μm. The number in each bar represents the number of neurites measured. Error bars represent standard error of the mean (SE).

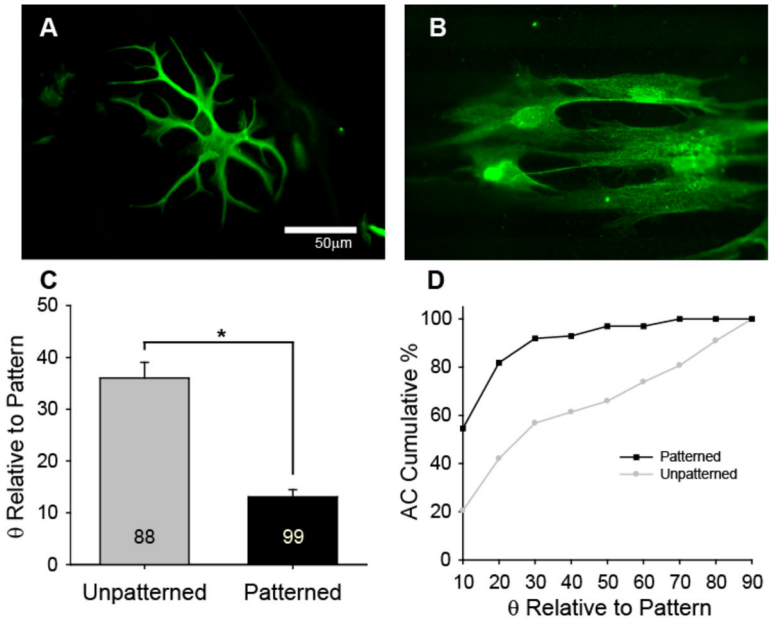

Figure 6.

AC alignment on unpatterned and patterned substrates. **A–B)** ACs demonstrate typical morphology on unpatterend polymers (A), but elongate and align on patterned polymers (B). **C)** The alignment angle (mean±SE) of ACs on unpatterned substrates is statistically different from the alignment angle on patterned substrates (*$p < 0.005$, Mann-Whitney Rank Sum test). The number in each bar represents the number of ACs measured. **D)** Representation of the cumulative percent of ACs at or below the angle relative to the pattern direction indicated in the x-axis. 55% of ACs align to the pattern (angle of 10° or less) and greater than 90% of ACs are within 30° or less of the pattern direction. Micropatterns used for AC alignment have periodicities of 50 μm and channel amplitudes of 3 μm.

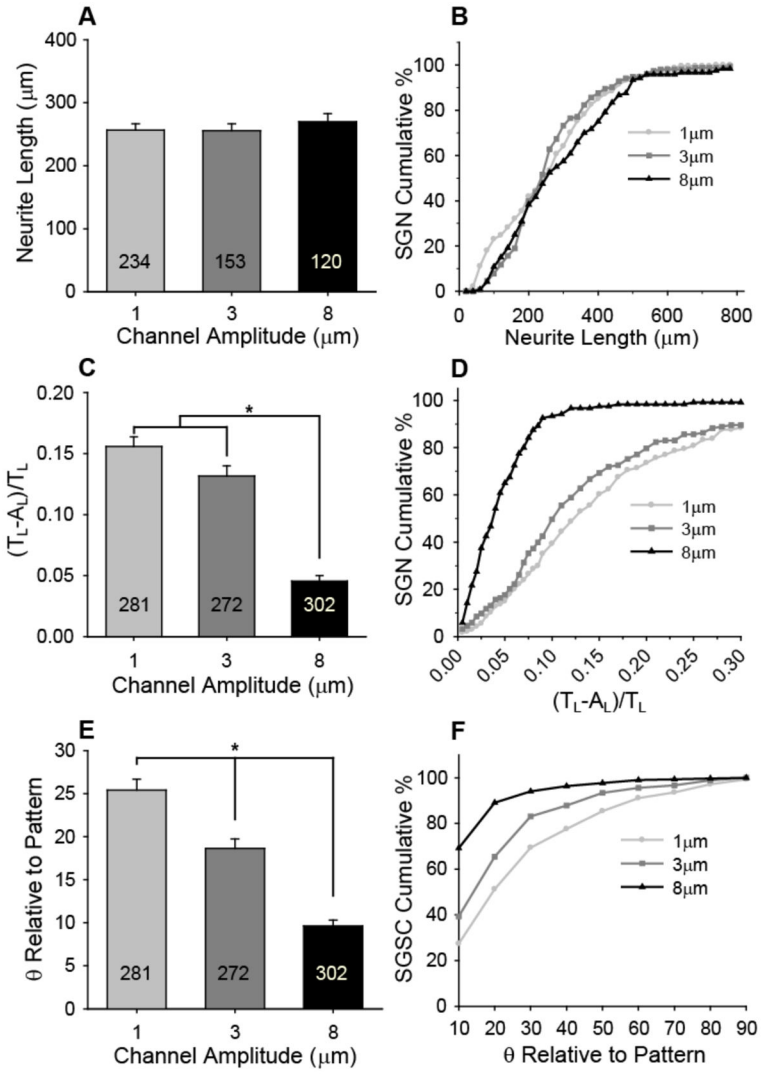

Figure 7.

SGN neurite and SGSC alignment on patterns with constant periodicity (50 μm) but varying amplitude. **A)** SGN neurite length is not statistically different when cultured on patterns that have channel amplitudes of 1, 3, and 8 μm. **B)** Representation of the cumulative percent of neurites at or below the length indicated in the x-axis. The spread of neurite lengths for the population of SGN neurites is also not affected by the given channel amplitudes. **C)** SGN neurite alignment (mean±SE) increases significantly with increasing channel amplitude (*$p < 0.005$, one way ANOVA). SGN neurite alignment was measured as a ratio of unaligned length per neurite length, $[(T_L - A_L)/T_L]$. Ratios that approach zero indicate the highest degree of alignment. **D)** Representation of the cumulative percent of neurites at or below the alignment ratio indicated in the x-axis. 93% of the SGN neurite population cultured on 8 μm deep channels falls within a low alignment ratio of 0.10 compared to 39% and 50% on 1 and 3 μm channels, respectively. **E)** SGSC alignment (mean±SE) increases significantly with increasing channel depth (*$p < 0.005$, one way ANOVA). SGSC orientation was measured as the angle between the pattern and the major axis of an ellipse fitted around the cell. **F)**

Representation of the cumulative percent of SGSCs at or below the angle relative to the pattern direction indicated in the x-axis. 70% of SGSCs align (i.e. angle of 10° or less) to patterns with channels that are 8 μm in amplitude compared to 30% and 40% that align to 1 μm and 3 μm deep channels, respectively.

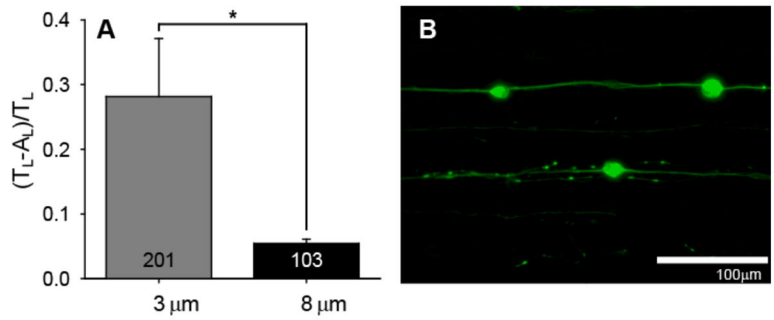

Figure 8.

DRGN neurite alignment on patterns with constant periodicity (50 μm) but varying amplitude. **A)** DRGN neurite alignment (mean±SE) increases significantly with increasing channel amplitude (*$p < 0.005$, one way ANOVA). DRGN neurite alignment was measured as a ratio of unaligned length per neurite length, $[(T_L - A_L)/T_L]$. **B)** Dissociated neurite growth from DRGNs on a pattern with 8 μm deep channels and a 50 μm periodicity. DRGN primary neurites and their branches strongly align to the pattern direction on 8 μm deep channels compared to the spread of neurite growth near the cell body on 3 μm deep channels (Fig 4C).

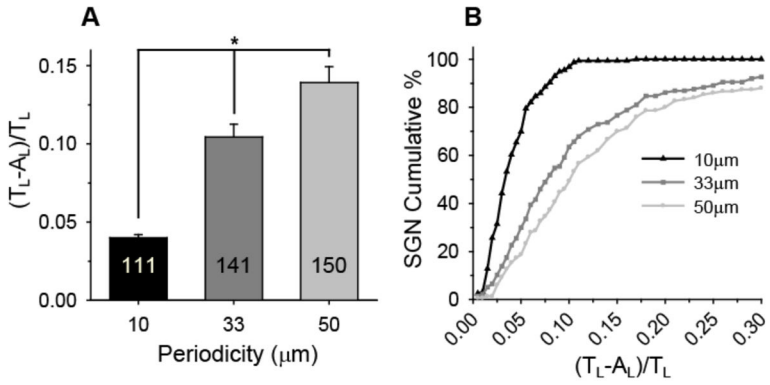

Figure 9.

SGN neurite alignment on patterns with constant amplitude (1 μm) but varying periodicity. **A)** SGN neurite alignment (mean±SE) increases significantly with decreasing periodicity (*$p < 0.005$, one way ANOVA). SGN neurite alignment was measured as a ratio of unaligned length per neurite length, $[(T_L-A_L)/T_L]$. **B)** Representation of the cumulative percent of neurites at or below the alignment ratio indicated in the x-axis. 97% of the SGN neurite population cultured on patterns with a 10 μm periodicity falls within a low alignment ratio of 0.10 compared to 63% and 49% on patterns with 33 and 50 μm periodicities, respectively.

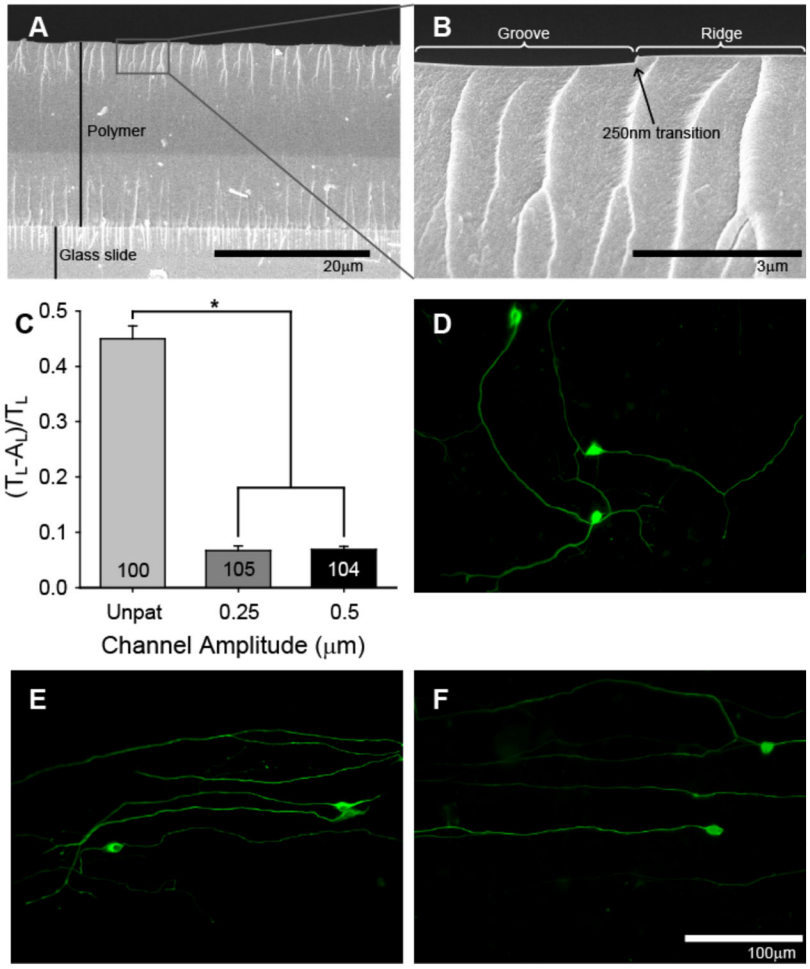

Figure 10.

SGN neurite alignment to nano-scale (<1 μm) features. **A–B)** Cross-sectional SEM images demonstrate the depth of the pattern features compared to the thickness of the polymer film. **C)** SGN neurites strongly align to patterns with 10 μm periodicities and 250 nm and 500 nm amplitudes (*$p < 0.005$, one way ANOVA). **D)** SGN neurite growth extends randomly on unpatterned HMA-co-HDDMA polymers. **E–F)** SGN neurite growth strongly aligns to patterns with 10 μm periodicities and 250 nm amplitudes (E) as well as to patterns with 50 μm periodicities and 8 μm amplitudes (F). Interestingly, there is no statistical difference ($p = 0.369$) between SGN neurite alignment on the patterns described in E and F. Cultures were stained with anti-NF200 antibodies (D–F). The pattern is oriented horizontally

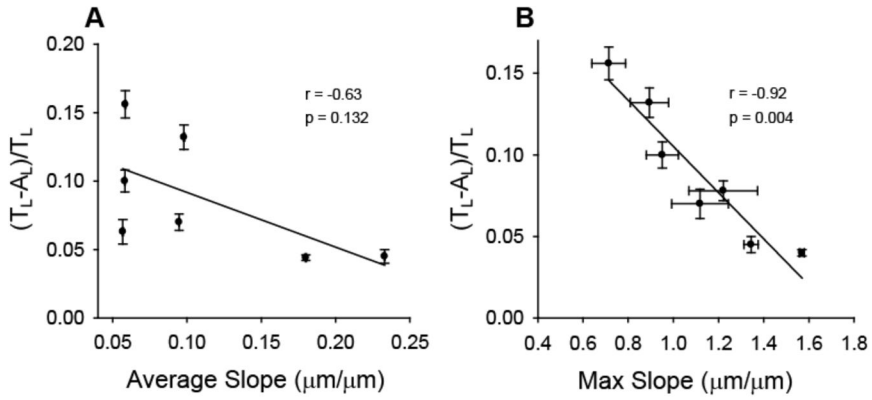

Figure 11.

Linear regression correlation of SGN neurite alignment with average (A) and maximum slope (B) of groove-ridge transitions. SGN neurite alignment strongly correlates with maximum feature slope. POINTS AND ERROR BARS ARE GIVEN IN TABLE 1

Table 1

Summary of micropattern dimensions, transitional slope, and neurite alignment

Periodicity (μm)	Amplitude* (μm)	Avg Slope* (μm/μm)	Max Slope* (μm/μm)	$(T_L-A_L/T_L$** (μm/μm)
10	0.25±0.01	0.057±3e-4	1.12±0.13	0.063±9e-3
10	0.51±0.02	0.095±2e-4	1.22±0.15	0.070±6e-3
10	1.02±0.1	0.180±4e-4	1.57±0.01	0.044±2e-3
33.3	1.07±0.1	0.058±2e-4	0.90±0.07	0.100±8e-3
50	1.04±0.1	0.059±2e-4	0.74±0.07	0.156±9e-3
50	3.1±0.3	0.098±4e-4	0.89±0.09	0.132±9e-3
50	8.1±0.8	0.233±2e-4	1.37±0.23	0.045±5e-3

* mean±SD

** mean±SE